

Structure and electronic properties of iron oxide clusters: A first-principles study

Sinhué López* and A. H. Romero†

CINVESTAV-Queretaro, Libramiento Norponiente No 2000, Real de Juriquilla, 76230 Queretaro, México

J. Mejía-López‡

Facultad de Física, Pontificia Universidad Católica de Chile, Casilla 306, Santiago 22, Chile

J. Mazo-Zuluaga§ and J. Restrepo||

*Grupo de Magnetismo y Simulación and Grupo de Instrumentación Científica y Microelectrónica,**Instituto de Física, Universidad de Antioquia, A.A. 1226, Medellín, Colombia 229*

(Received 12 September 2008; published 13 August 2009)

In this study we present results of electronic structure calculations for some iron oxide clusters of the form Fe_nO_m on the basis of the GGA+ U approximation. The cluster size ranged between 33 and 113 atoms corresponding to length scales between around 7 Å and 12 Å in diameter, respectively. Initial atomic configurations before relaxation were created by considering two different space groups corresponding to the cubic $Fd\bar{3}m$ and monoclinic $P2/c$ symmetries. The charge and the magnetization per atom were computed. In particular, the charge distribution of the cluster relaxed from cubic symmetry and containing 113 atoms reveals a well-defined periodic pattern of Fe pairs consistent with a partial charge-ordering scenario. Results evidence that the ground-state cohesive energy is smaller in the clusters originated from the $P2/c$ symmetry. This fact indicates that at least in the largest cluster, having more tendency to preserve the initial structure, the low-temperature monoclinic phase is energetically more stable. Clusters starting from monoclinic symmetry are characterized by an insulating state, whereas those optimized from cubic symmetry exhibit a very small electronic gap. Finally, radial and angular distribution functions reveal strong modifications of the starting crystalline structures after relaxation with a tendency of forming cage-like structures.

DOI: [10.1103/PhysRevB.80.085107](https://doi.org/10.1103/PhysRevB.80.085107)

PACS number(s): 73.22.-f, 71.15.Mb, 75.75.+a, 61.46.Bc

I. INTRODUCTION

In the last two decades, the progress in the development of some experimental techniques and theoretical tools, has allowed to take a look on the different fundamental properties of clusters containing few atoms (dimers, trimers, etc.) up to tens of atoms. The increasing importance on this issue is related to the fact of understanding how the different properties evolve as individual atoms are brought together to form nanostructures, solids, and to investigate the minimum size at which clusters begin to exhibit similar properties of the corresponding bulk systems. Clusters are also excellent candidates to explore the nature of the chemical bond and the influence of the so-called finite-size effects on the electronic structure and also the magnetic properties in clusters containing magnetic atoms. On this last respect, iron oxide clusters have attracted the attention as long as the Fe-O interaction is one of the most important in nature due to the variety of molecules or complexes containing Fe-O bonds as can be evidenced for instance in some phenomena such corrosion. As concerns to practical applications, some iron oxide clusters such as Fe_2O_3 seem to be potential candidates for CO oxidation and NO reduction which are undesirable products in many industrial processes and their removal is one of the most important environmental problems nowadays.^{1,2} A systematic study on iron oxide clusters of the form FeO_y and Fe_2O_y for different oxygen contents, and being Fe_2O_5 the largest cluster, was carried out using anion photoelectron spectroscopy.^{3,4} A near linear increase in the electron affinity with the number of oxygen atoms was found consistent with

ionic bonding as expected in metal oxides and with a charge transfer picture where the electrons are sequentially transferred from the Fe atoms to the O atoms. Production and characterization of small oxide clusters under well-controlled conditions have been also carried out in previous works dealing with Fe_nO and Fe_nO_2 clusters.^{5,6} Bigger iron oxide (Fe_mO_n) clusters up to a maximum size of $\text{Fe}_{30}\text{O}_{32}$ have been also generated by means of laser ablation of the metal and reaction with various concentrations of O_2 in He.⁷ Several compositions involving equiatomic, oxygen rich, and oxygen deficient cluster series could be produced by controlling the oxygen concentration in the system. Theoretical findings like those reported by Jones *et al.*⁸ have provided evidence for the existence of single hollow rings structures for equiatomic Fe_nO_n ($n=2-5$) clusters contrary to the compact NaCl structure of bulk FeO. Above $n=5$, clusters assemble to form more complex structures such as decorated and undecorated nanotowers giving rise to new kinds of nanostructures. Their maximum cluster size was $\text{Fe}_{12}\text{O}_{13}$ and to the best of our knowledge no theoretical studies on larger iron oxide clusters have been reported. Results revealed a trend consisting of an increase in the bond length, including values as large as 2.15 Å, as the cluster size increases, whereas the gap energy exhibits a fluctuating behavior. Other clusters like Fe_{13}O_2 can exhibit bond lengths as large as 2.36 Å and they are characterized by moment reduction as compared to Fe_{13} clusters.⁹ The case of Fe_{13}O_8 is very interesting and it is one of the so-called magic clusters accordingly with the largest values of binding energies. These clusters have been produced by using a reactive laser vaporized cluster source and

it has been also studied by using density-functional theory (DFT) in the framework of the conjugate-gradient iterative minimization technique.¹⁰ Structure optimization from two different initial configurations gave rise to structures both of them characterized for having an Fe central atom with the others forming a cage with an Fe-O interatomic distance between the central atom and an oxygen in the surroundings surprisingly large, i.e., 3.087 Å and 3.141 Å in the two cases. Magnetic and vibrational calculations of this magic cluster have been also performed on the basis of an all-electron DFT.¹¹ Results revealed a structure characterized also by a central Fe atom and a distance Fe-O relative to the central atom of 3.31 Å and a total moment of $32\mu_B$ when considering a ferromagnetic state. If ferrimagnetic coupling is considered, clusters are characterized by an Fe-O distance relative to the central atom of 3.23 Å and a total moment of $14\mu_B$. Other magic transition-metal oxide clusters have been also reported to occur.¹²

On the other hand, as is well established, the magnetic and electronic properties are strongly dependent on the specific atomic surface reconstruction as it has been studied in iron oxides such as magnetite by using DFT with the GGA+ U and LDA+ U approaches.¹³ Thus, the fact of being able to tailor the properties of small clusters by changing size and composition like the proportion of Fe and O atoms, as concerns to Fe_nO_m clusters, has motivated us to consider this kind of clusters. The purpose of this article is to characterize from different perspectives (electronic, magnetic, and structural) iron oxide clusters of the form Fe_nO_m when these are constructed on the basis of a well-studied iron oxide such as magnetite (Fe_3O_4) and starting from the two different space groups ascribed to this material, namely cubic ($Fd\bar{3}m$) and monoclinic ($P2/c$), which correspond to the structures of bulk magnetite above and below the Verwey temperature, respectively.^{14,15} In this work we report on Fe_nO_m clusters having 33, 45, and 113 atoms corresponding to the following stoichiometries $Fe_{17}O_{16}$, $Fe_{17}O_{28}$, and $Fe_{45}O_{68}$. Finally, we want to stress that to the best of our knowledge, no first-principles studies on Fe_nO_m clusters having several tens of atoms have yet been reported.

II. COMPUTATIONAL DETAILS

Electronic structure and density of state (DOS) calculations were performed using DFT (Ref. 16) in the framework of the GGA+ U approach on the basis of the Dudarev's method¹⁷ and using the PW91 pseudopotential for the exchange-correlation functional with the Vosko-Wilk-Nusair correction.¹⁸ Calculations were also performed in the framework of the projector augmented wave method^{19,20} as implemented in the VASP package.²¹ The on-site Coulomb term has been included according to the degree of localization of the Fe d electrons. We set the U parameter to 4.5 eV for Fe cations, which is based on constrained calculations.^{15,22–24} On this last respect, we want to stress that LDA+ U band structure calculations with U varying from 4 to 6 eV provide optical, magneto-optical and x-ray magnetic circular dichroism spectra in reasonable agreement with experimental data.²³ The Hund's coupling for Fe was set to

$J=0.89$ eV.^{15,25} Both, the U and J parameters for oxygen were set to zero. In any case, we should stress that there is a delicate balance between U and J which in principle can lead to differences regarding the final magnetic state of the system. Therefore, we have decided to choose the parameters already used and reported in the literature, where good agreement of a large diversity of properties have been reported. Clusters were simulated by periodic cells separated by a sufficiently high amount of vacuum in order to avoid intercluster interactions. Hence, our simulated system can be considered as a periodic and monodisperse array of isolated clusters. Two different initial crystalline structures, namely $Fd\bar{3}m$ and $P2/c$ and three different cluster sizes having 33, 45, and 113 atoms were considered corresponding to $Fe_{17}O_{16}$, $Fe_{17}O_{28}$, and $Fe_{45}O_{68}$ clusters. Hereafter, such clusters are labeled in generic form as $C33$, $C45$, and $C113$; and as $C33F$, $C33P$, $C45F$, $C45P$, $C113F$, and $C113P$, where F and P stand for the initial $Fd\bar{3}m$ and $P2/c$ symmetries, respectively. These amounts yield the following average diameters in the relaxed structures: 7.0(1), 8.2(1) and 12.3(1) Å. The lateral parameter of the supercell was set to 18 Å, 20 Å, and 24 Å for $C33$, $C45$, and $C113$ clusters, respectively. A Wigner-Seitz radius $r_{WS}=1.302$ Å for iron and $r_{WS}=0.82$ Å for oxygen were used. The energy cutoff for the plane wave representation was 500 eV. The convergence force criterion was set to 0.01 eV/Å per atom. The charge of each atom was estimated by using the Bader method, where a fair partition of the electronic charge is performed by only including the valence electrons. Details of the implementation and the meaning can be found in Henkelman *et al.*²⁶ This method has been used to calculate the partial charges in H and O atoms on the H_2O molecule, and in crystals such as NaCl and MgO,²⁶ where an interpretation of the electronic charge transfer has been discussed. The magnetic moment distribution was computed by integrating the electronic density within the Wigner-Seitz radius for each atom. The overall magnetization μ_{WS} per cluster were also determined by summing the respective quantities per atom. Cohesive energy per one formula unit was also computed according to $E_{coh}=E_{tot}-nE_{Fe}-mE_O$ where n and m correspond to the number of Fe and O atoms with energies in the isolated state E_{Fe} and E_O , respectively. Only for comparison purposes, the structural and electronic properties of bulk magnetite, taken as reference material, have also been computed. In this case, a $6\times 6\times 6$ Monkhorst-Pack²⁷ grid and a total number of 28 k points in the irreducible Brillouin zone were employed for the $Fd\bar{3}m$ symmetry, whereas a $6\times 6\times 2$ Monkhorst-Pack grid with 36 k points for $P2/c$ symmetry was considered. A Gaussian smearing factor of 0.01 for clusters and monoclinic bulk was employed, whereas the Methfessel-Paxton method was used for the cubic bulk.²⁸ For clusters, calculations were done at the Γ point. Finally, in order to perform a structural analysis before and after the optimization process, both the radial [RDF or $g(r)dr$] and angular [ADF or $h(\theta)d\theta$] distribution functions were computed. To compute RDF, a cut-off distance r_c approximately equals to the cluster diameter was considered. This function accounts for the number of neighbors surrounding every atom at a given distance between r and $r+dr$, where $0\leq r\leq r_c$. To compute ADF, angles formed

TABLE I. Ground-state lattice and electronic properties for the cubic $Fd\bar{3}m$ and monoclinic $P2/c$ structures of bulk magnetite. Average magnetization per one formula unit (m_{av}) are given in μ_B . Lattice constants (a, b, c) are in Å, cohesive energy (E_{coh}) per formula unit and gap (Δ_g) in eV.

Phase	Quantity	This work	Piekarz ^a	Exp.
$Fd\bar{3}m$	a	8.456	8.446	8.394 ^b
	E_{coh}	-35.791		
	m_{av}	3.825	3.96	4.05 ^c
	Δ_g	0	0	0
	$P2/c$	a	6.013	5.967
$P2/c$	b	6.017	5.995	5.925 ^b
	c	16.865	17.034	16.775 ^b
	β	90.230	90.417	90.237 ^b
	E_{coh}	-36.115		
	Δ_g	0.25	0.33	0.14 ^d

^aReference 14.

^bReference 29.

^cReference 30.

^dReference 31.

by triads of atoms within spheres of 2.2 Å were considered. Finally, we have calculated a mean coordination number according to the following proposed relationship

$$\langle z(r) \rangle = \frac{1}{N} \sum_{r_i \in [r, r+dr]} \sum_{j=1}^N \delta(r_i - r_j), \quad (1)$$

where N is the total number of atoms and \mathcal{N}_r is the number of atoms at a distance r_i belonging to the interval $[r, r+dr]$. This mean value was computed by considering the total number of neighbors per atom within the entire cluster. Histograms showing the way as the atoms become spatially distributed were also computed. These quantities allows having a full structural characterization of the clusters.

III. RESULTS AND DISCUSSION

In Table I we show the ground-state lattice and electronic properties for $Fd\bar{3}m$ and $P2/c$ structures of bulk magnetite, our reference material, obtained in the present calculations. Experimental data and theoretical results by Piekarz *et al.*¹⁴ are also listed for comparison. Results show an overall good agreement with experimental data of Refs. 29–31 and with those of Piekarz *et al.*,¹⁴ wherever available. It must also be noticed that the ground-state cohesive energy of the crystal E_{coh} per one formula unit is much smaller in the $P2/c$ phase than in the $Fd\bar{3}m$ phase, indicating that the low temperature monoclinic phase of $P2/c$ symmetry is the most stable. This fact agrees with several results in the literature where the monoclinic phase has been reported as the lowest-energy state.^{14,15,29} Data corresponding to charge and magnetization per atom for both phases are listed in Table II. In the case of the cubic phase, different labels (B1, B2, B3) have been employed to compare the parameters associated to iron cat-

TABLE II. Valence electric charge (Q) in e units and magnetic moments per atom (μ) in μ_B , for the cubic $Fd\bar{3}m$, and monoclinic $P2/c$ structures of bulk magnetite.

Space group	Index	Atom	$Q(e)$	$\mu(\mu_B)$
$Fd\bar{3}m$	1,2	Fe _A	1.49 ± 0.01	-4.02
	3,5	Fe(B1)	1.50 ± 0.02	3.92
	4	Fe(B2)	1.47	4.02
	6	Fe(B3)	1.51	3.83
$P2/c$	1,2,6,8	Fe _A	1.19 ± 0.05	-4.02
	3–5,7	Fe _A	1.46 ± 0.04	-4.02
	9,16,21	Fe _B	1.65 ± 0.03	3.65 ± 0.01
	10,15,18,20,23	Fe _B	1.56 ± 0.01	3.66 ± 0.01
	11,14,17	Fe _B	1.94 ± 0.03	4.12 ± 0.01
	12,13,19,22,24	Fe _B	1.85 ± 0.03	4.12

ions in octahedral sites under bulk conditions with those corresponding to clusters. Charge and moment distribution reveal therefore the occurrence of three different octahedral Fe sites for the $Fd\bar{3}m$ space group, whereas two different tetrahedral Fe sites and four nonequivalent B -Fe sites are found for the $P2/c$ symmetry. We find these last numbers in accord with previous results where two distinct A -Fe sites and four independent octahedral B -site iron atoms were concluded from structural refinement of stoichiometric single crystals of magnetite using high-resolution x-ray and neutron powder diffraction.²⁹ Regarding the magnetic structure for the $P2/c$ symmetry, while the total moment per one formula unit remains at $\sim 4\mu_B$ the iron magnetic moments amount to $-4.02\mu_B$ for A sites and between $3.65\mu_B$ and $4.13\mu_B$ for B sites. It must be stressed however that the magnetic moment is not a well-defined quantity in non absolute ionic crystalline systems as far as it can be partitioned depending on the chosen value for r_{WS} . By using our value of 1.302 Å we find numerical results in rather good agreement with some others found in literature.^{14,15,32–35} However, it is interesting to point out that, in particular, the corresponding values for an A -Fe site are very different from the value of $5\mu_B$ derived from Hund's rules and the nominal Fe^{3+} charge on a typical A site. This fact is consistent with the itinerant nature of magnetism in this system and with changes in the valence states. Differences in sign are consistent with an antiparallel alignment between A and B sublattices in agreement with a ferrimagnetic state.

Concerning clusters, Table III shows the results corresponding to the cohesive energy and the magnetization μ_{WS} . By comparing the corresponding energy values we can conclude that the ground-state phase is that resulting from the initial $P2/c$ symmetry. As we will show later by comparing the radial and angular distribution functions before an after relaxation, the largest $C113$ cluster tends to preserve the starting configuration suggesting that the monoclinic phase is energetically more stable than the cubic phase in the low temperature regime. This result in addition to the fact that such cluster, namely $Fe_{45}O_{68}$ whose chemical formula can be written also as $Fe_{2,647}O_4$, is stoichiometrically similar to bulk

TABLE III. Global parameters derived from the present calculations for the relaxed $C33$, $C45$, and $C113$ magnetite clusters obtained from the initial $Fd\bar{3}m$ and $P2/c$ structures.

Phase	Cluster	E_{coh} (eV)	μ_{WS} (μ_B)
$Fd\bar{3}m$	33	-18.933	32.930
	45	-25.892	28.905
	113	-31.260	43.099
$P2/c$	33	-18.947	27.178
	45	-25.958	28.767
	113	-31.454	43.182

magnetite (Fe_3O_4), allows to suggest that magnetite nanoparticles should, in principle, exhibit Verwey transition. Such conclusion is also endorsed by the fact that the Verwey transition has also been observed in highly nonstoichiometric magnetite of the form $\text{Fe}_{3-\delta}\text{O}_4$.³⁶

In clusters with $P2/c$ symmetry, the total magnetization increases as the cluster size is increased. However, this is not strictly the case for clusters with $Fd\bar{3}m$ symmetry where the total magnetization of the smallest cluster ($C33$), is greater than that of $C45$. This fact is due to a parallel alignment of one of the A spins respect to the B spins (see Table IV) giving rise to a ferromagnetic state.

Figures 1 and 2 show the resulting atomic and charge distribution for the relaxed clusters starting from symmetries $Fd\bar{3}m$ and $P2/c$, respectively. Results corresponding to charge and magnetic moment per atom are listed in Tables IV and V for $C33F$ and $C33P$ respectively, whereas those for $C45F$ and $C45P$ are listed in Tables VI and VII, respectively. From these results several features are remarkable. First, all clusters, including $C113$, are characterized for having a single Fe_A ion located at the center of the cluster with the rest of ions in the surroundings giving rise to a cagelike structure. In the case of $C33$, this Fe_A ion is labeled as $N_i=5$ [the corresponding in the bulk is $\text{Fe}_A(2)$] in the cubic phase and as $N_i=2$ [the corresponding in the bulk is $\text{Fe}_A(1)$] in the monoclinic phase (Tables IV and V). Such cation in the cluster exhibits a loss of charge accompanied by an increase in the magnetic moment relative to the corresponding atom in the bulk. Surprisingly, only in the $C33F$ cluster, such central

TABLE IV. Valence electric charge and magnetic moment per atom for $C33F$. The units for charge and magnetization are e and μ_B , respectively. N_i stands for the index employed in labeling the atoms within the cluster, whereas the corresponding positions in the bulk are indicated in parentheses.

N_i	Atom	Q_i	μ_i	Color
1-4	$\text{Fe}_A(1)$	1.99 ± 0.04	-3.62	green
5	$\text{Fe}_A(2)$	0.38	2.90	red
6,7,10,13,16,17	$\text{Fe}(B1)$	-0.40 ± 0.02	3.62	blue
8,11,14	$\text{Fe}(B2)$	-0.39	3.62	blue
9,12,15	$\text{Fe}(B3)$	-0.39 ± 0.02	3.62	blue

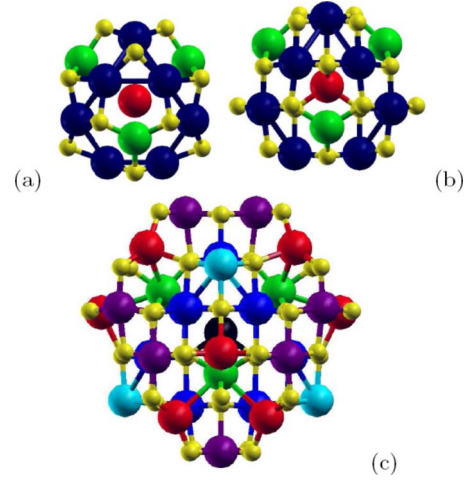


FIG. 1. (Color online) Optimized structures and valence electric charge distribution of the relaxed clusters originated from symmetry $Fd\bar{3}m$ corresponding to (a) $C33F$, (b) $C45F$, and (c) $C113F$. Light gray (yellow) small balls correspond to oxygens, black (dark blue) for Fe_B ions (and dark gray (purple) in the case of $C113F$), whereas Fe_A ions are represented by light gray (green) and (gray) red spheres (and a central black sphere in the case of $C113F$). Different colors correspond also to different charge and magnetization per atom values as described in Tables IV, VI, and VIII.

moment exhibits a parallel alignment respect to those spins of the B sublattice giving rise to a partial ferrimagnetic state different from the expected full ferrimagnetic behavior (antiparallel alignment of the moments from the A and B sublattices). This scenario is the one responsible for the large value of the total magnetization observed for $C33F$. The interaction between the central atom with the rest is weak but non-negligible. For example, if the cohesive energy for that particular atom in the $C33F$ cluster is calculated ($E_{33}-E_{32}$

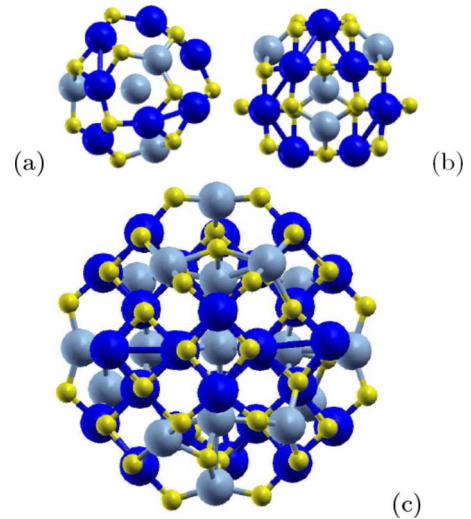


FIG. 2. (Color online) Optimized structures and valence electric charge distribution of the relaxed clusters originated from symmetry $P2/c$ corresponding to (a) $C33P$, (b) $C45P$, and (c) $C113P$. Light gray (yellow) small balls correspond to oxygens, black (dark blue) for Fe_B ions, and gray (light blue) for Fe_A ions.

TABLE V. Valence electric charge and magnetic moment per atom for $C33P$. The units of charge and magnetization are e and μ_B , respectively. N_i stands for the index employed in labeling the atoms within the cluster, whereas the corresponding positions in the bulk are indicated in parentheses.

N_i	Atom	Q_i	μ_i
1,4,5	Fe _A (3)	1.02 ± 0.09	-3.62
2	Fe _A (1)	0.55	-2.98
3	Fe _A (3)	0.66	-3.62
6	Fe _B (9)	0.67	3.63
9	Fe _B (9)	1.35	3.63
10	Fe _B (9)	1.14	3.63
7	Fe _B (11)	0.93	3.63
8,12,15,16	Fe _B (12)	1.21 ± 0.06	3.63
11	Fe _B (11)	0.68	3.63
13,14	Fe _B (10)	1.31 ± 0.02	3.62
17	Fe _B (10)	0.74	3.62

$-E_1$), a value of 1.67 eV is obtained, whereas a 6.74 eV value is obtained for the $C45F$ cluster. Therefore, we can conclude that even though the central atom is bound to their neighbors, there is an electronic interaction between the central atom and the rest of the cluster. This fact can be also deduced from the spacial distribution of the electronic density curves shown in Fig. 3(a) as two-dimensional projections along different planes. The slight distortion in the density curves around the central atom due to the presence of its surroundings neighbors endorse the occurrence of such a weak interaction. The degree of distortion is greater for larger clusters [e.g., $C45P$, Fig. 3(b)]. The rest of Fe cations, forming the cluster surface and representing the 97% of the total, are characterized by an increase in the electric charge relative to the corresponding atoms embedded in the bulk (all the ΔQ_i , defined as $Q_i - Q_{\text{bulk}}$, are positive). The same conclusion is valid if the charge values are compared to those of the free atoms ($Q_i - q$). Results evidence therefore a charge transfer process between Fe and O cations. It must be stressed that despite the electric charge of oxygens atoms is not shown in the tables, the corresponding ΔQ_i were negative. Charge transfer is also observed for $C45$ and $C113$ clusters independently of what the starting symmetry was and

TABLE VI. Valence electric charge and magnetic moment per atom for $C45F$. The units of charge and magnetization are e and μ_B , respectively. N_i stands for the index employed in labeling the atoms within the cluster, whereas the corresponding positions in the bulk are indicated in parentheses.

N_i	Atom	Q_i	μ_i	Color
1-4	Fe _A (1)	1.47	-3.69	green
5	Fe _A (2)	2.03	-3.84	red
6,7,10,13,16,17	Fe(B1)	1.61	3.71	blue
8,11,14	Fe(B2)	1.61	3.71	blue
9,12,15	Fe(B3)	1.61	3.71	blue

TABLE VII. Valence electric charge and magnetic moment per atom for $C45P$. The units of charge and magnetization are e and μ_B , respectively. N_i stands for the index employed in labeling the atoms within the cluster, whereas the corresponding positions in the bulk are indicated in parentheses.

N_i	Atom	Q_i	μ_i
1	Fe _A (3)	1.20	-3.66
2	Fe _A (1)	1.61	-3.84
3,5	Fe _A (3)	1.32 ± 0.05	-3.65
4	Fe _A (3)	0.37	-3.66
6,10	Fe _A (9)	1.71 ± 0.06	3.45
7	Fe _B (11)	0.94	3.43
8	Fe _B (12)	1.75	4.13
9	Fe _B (10)	1.21	4.12
11	Fe _B (11)	1.32	4.13
12	Fe _B (12)	1.86	3.43
13,14	Fe _B (10)	1.77 ± 0.05	3.47
15	Fe _B (12)	1.68	3.46
16	Fe _B (12)	1.59	3.50
17	Fe _B (10)	1.85	3.50

with a marked tendency of the surface Fe atoms to increase their electric charge. It can be concluded so far that a reordering of the charge and magnetic moment occurs as the system size decreases to nanoscale.

We have also calculated the total DOS of the relaxed clusters and bulk magnetite. Zero energy was defined occurring at the Fermi level. Under bulk conditions and $Fd\bar{3}m$ symmetry, magnetite exhibits a metallic behavior ($\Delta_g = 0$) with the Fermi level sitting in the middle of the spin-down Fe(B) t_{2g} band (Fig. 4). Figure 5 shows the opening of an energy gap Δ_g at the Fermi level as the cubic structure is transformed

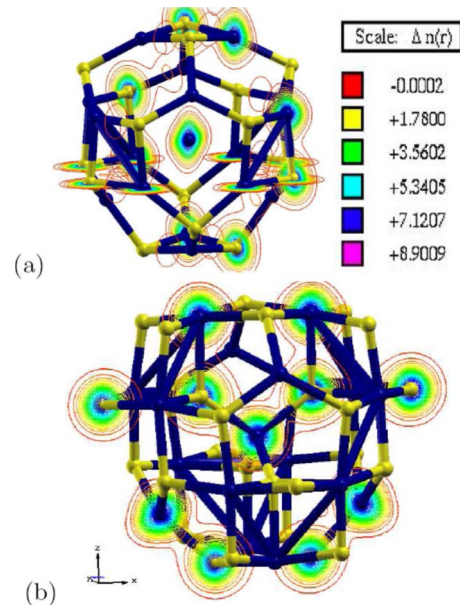


FIG. 3. (Color online) Two-dimensional projections of the electronic density curves for (a) $C33F$ and (b) $C45P$.

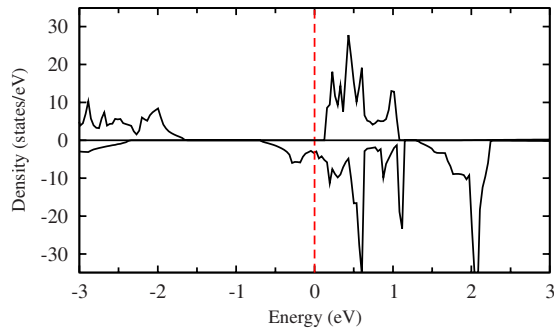


FIG. 4. (Color online) Total electron DOS for the spin-up (top) and spin-down (bottom) electrons in bulk magnetite with cubic $Fd\bar{3}m$ symmetry. The Fermi level is at zero energy.

into the monoclinic structure. This gap (0.25 eV), giving rise to an insulating state, is larger than the experimental value of 0.14 eV obtained by optical measurements at $T=10$ K,³¹ but is close to the values obtained in other electronic structure calculations.^{14,15,30,37} As concerns to the clusters, it is evident the discrete character of the energy levels arising from two contributions, atomic electron levels, and bonding states coming from hybridized orbitals. Figures 6 and 7 show the total DOS of the relaxed $C113$ clusters for the two considered initial structures. Zero energy was defined occurring at the highest occupied molecular orbital. By comparing with those results under bulk conditions, the signature of a metallic behavior is still preserved for $C113F$, whereas in the case of $C113P$ the width of the band gap in the minority spin channel increases to 0.3 eV reinforcing the onset of an insulating state. The scenario is more complex for smaller clusters, namely $C33$ and $C45$, where is difficult to identify a band gap due to the discrete character of the energy levels. Despite that, it is possible however to infer an energy gap whose size dependence is not monotonous according to the nonmonotonous Fe:O ratio in the studied clusters. In any case, the width of the gap in the minority spin channel for $C33P$ and $C45P$ clusters was estimated around 1 eV reinforcing even more the insulating state.

Figure 8 shows the charge distribution for the $C113F$ cluster. Results reveal a charge and magnetic moment reordering relative to the bulk. Such a reordering gives rise to an increase in the number of nonequivalent Fe atoms from four

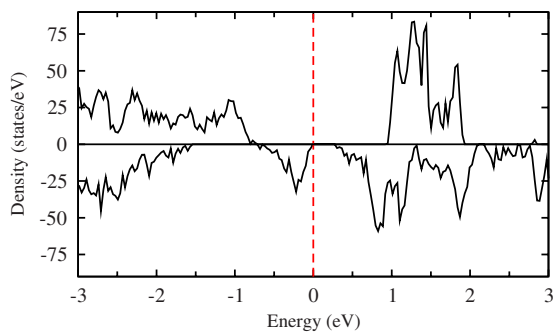


FIG. 5. (Color online) Total electron DOS for the spin-up (top) and spin-down (bottom) electrons in bulk magnetite with monoclinic $P2/c$ symmetry. The Fermi level is at zero energy.

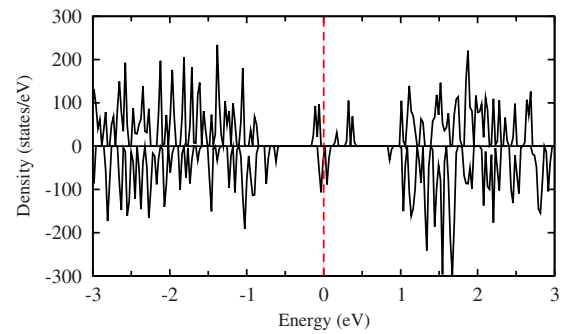


FIG. 6. (Color online) Total electron DOS for the spin-up (top) and spin-down (bottom) electrons for $C113F$ clusters.

(in the bulk) to six (in the cluster), as can be deduced from Table VIII. Such a reordering scenario is characterized by the presence of Fe pairs on the surface having both the same charge ($1.80 \pm 0.03e$) and the same magnetic moment per atom ($3.72\mu_B$). The formation of such dimers, consistent with a charge-ordering scenario, has been already reported to occur in magnetite on the basis of the so-called bond dimerization model.^{15,38} Regarding the magnetic structure, the iron magnetic moments amount between $-3.97\mu_B$ and $4.11\mu_B$. Different from this, $C33F$ and $C45F$ clusters are characterized only by three nonequivalent iron atoms. The number of such nonequivalent Fe atoms increases dramatically for those clusters originated from $P2/c$ symmetry. In the case of $C113P$ clusters, that number is as bigger as 30 indicating a high degree of disorder as concerns to charge and magnetic moment distribution.

Variations in charge and magnetization, relative to the bulk, have also been analyzed as a function of the position of the atoms relative to the center of the cluster. The corresponding results for $C33F$ are shown in Figs. 9 and 10. For this cluster size there is a clear tendency of the average charge to increase from the center to the surface. Contrary to this, the average magnetization decreases in the same direction and a linear relationship between the mean values $\langle \Delta Q \rangle$ and $\langle \Delta \mu \rangle$ can be inferred. Analogously, a linear relationship is also obtained for $C45F$. Such a well-behaved dependence, holding only for the smallest clusters, is not longer observed for $C113F$ where such quantities seem to be uncorrelated. This fact can presumably be ascribed to a higher degree of disorder due to the increase in nonequivalent iron sites hav-

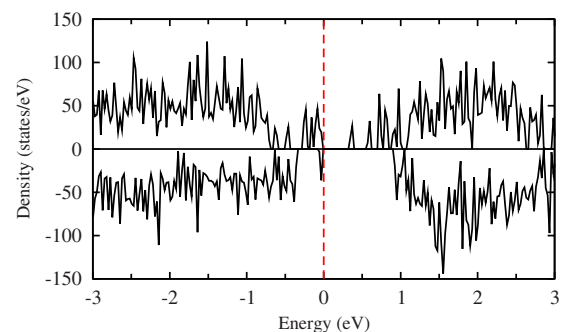


FIG. 7. (Color online) Total electron DOS for the spin-up (top) and spin-down (bottom) electrons for $C113P$ clusters.

TABLE VIII. Valence electric charge and magnetic moment per atom for $C113F$. The units of charge and magnetization are e and μ_B , respectively. N_i stands for the index employed in labeling the atoms within the cluster, whereas the corresponding positions in the bulk are indicated in parentheses.

N_i	Atom	Q_i	μ_i	Color
1,3–9,11,13,16,17	$Fe_A(2)$	1.29 ± 0.04	-3.96	red
2,10,12,14	$Fe_A(1)$	1.62 ± 0.01	-3.92	green
15	$Fe_A(2)$	1.64	-3.97	black
18–20	$Fe(B2)$	1.79 ± 0.01	3.72	purple
24,28	$Fe(B2)$	1.54	4.11	blue
35	$Fe(B2)$	1.37	4.11	blue
45	$Fe(B2)$	1.39	3.58	cyan
21	$Fe(B3)$	1.38	3.58	cyan
25	$Fe(B3)$	1.37	4.11	blue
32,42	$Fe(B3)$	1.52 ± 0.01	4.11	blue
39–41	$Fe(B3)$	1.80 ± 0.03	3.72	purple
22,23,27,33,43,44	$Fe(B1)$	1.45 ± 0.08	4.11	blue
26,34	$Fe(B1)$	1.38 ± 0.01	3.58	cyan
29–31,36–38	$Fe(B1)$	1.80 ± 0.03	3.72	purple

ing the same charge and concomitantly different values of the magnetic moment, which is not the case for smallest clusters.

As concerns to the structural characterization of the clusters, both the radial and angular distribution functions were computed. In Figs. 11 and 12 such functions for $C113P$ clusters before and after the relaxation process are displayed. In all cases the initial atomic positions used as input parameters were obtained from literature and they correspond to high-resolution structural refinement analysis of our reference material.²⁹ Due to the reduced number of atoms in these systems and the high degree of discreteness, each cluster represents a particular scenario with a particular structural signature resulting in different RDF and ADF functions. An important feature, common to all the clusters, independently of the initial space group, is the peaks broadening after relaxation which is more noticeable in monoclinic clusters. It must be stressed that the conditions and the step resolution (1.3 Å) were kept fixed in all cases. Thus, the broadening of peaks, associated to disorder, which is less marked in clusters originated from cubic symmetry, agrees with the greater

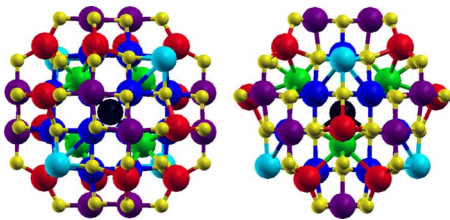


FIG. 8. (Color online) Valence electric charge distribution for $C113F$ clusters. Two different views of the cluster are displayed. Every color stands for a given set of charge and magnetic moment. Dimers are those represented by purple color corresponding to $6.95e$ and $3.72\mu_B$.

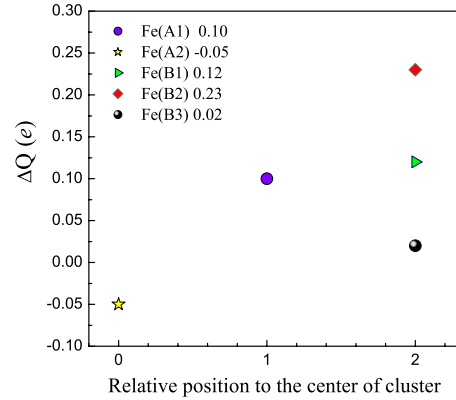


FIG. 9. (Color online) Variation of electric charge per atom relative to the bulk with the atomic position measured from the center for $C33F$ clusters. Numbers 1 and 2 along the x axis stand for first and second nearest neighbors, respectively.

amount of nonequivalent iron sites observed in clusters originated from monoclinic symmetry. Atomic displacements give rise also to a different distribution of angles and consequently to a peaks broadening in the ADF function. A remarkable feature is also the change in the cluster volume after relaxation. Volume was computed by considering a sphere of a radius equals to the distance, relative to the center, of the outermost atom. For $C113P$ a volume expansion from around 1039 \AA^3 to 1051 \AA^3 is observed, whereas a volume reduction from around 1002 \AA^3 to 985 \AA^3 takes place for $C113F$. Another particular interesting feature is the presence of a single atom very close to the geometrical center of the cluster with the rest of the atoms in the surroundings. This fact is easily visualized in Fig. 13 showing the distribution of atoms with the distance to the geometrical center of the cluster. As can be observed, atoms are located in groups of concentric layers separated by spaces in between, forming an onionlike structure. The thickness of such layers, which in turn corresponds to the peaks broadening observed in the RDF and ADF functions, depends on the distance and the type of cluster. A special case is the smallest cluster $C33$ with a single atom in the center and the remain-

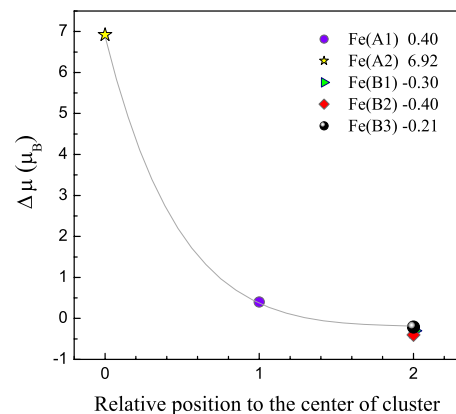


FIG. 10. (Color online) Variation of the magnetization per atom relative to the bulk with the atomic position measured from the center for $C33F$ clusters.

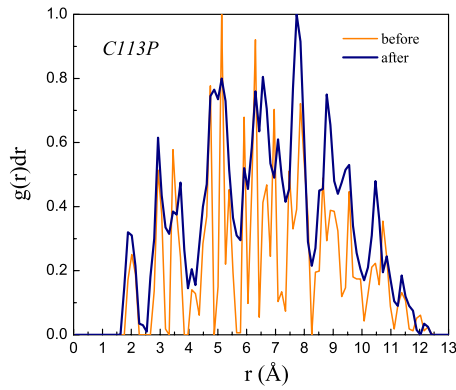


FIG. 11. (Color online) Radial distribution function for $C113P$, before and after relaxation.

ing distributed on the surface, which corresponds to 97% of the total of atoms. As the cluster size increases it turns out more difficult to realize what is exactly the surface (Figs. 13 and 14).

Figure 14 shows the histogram of the number of atoms and the mean coordination number (Eq. (1)) with the distance to the center of the cluster for $C113P$. As is observed, the mean coordination number decreases in a well-behaved fashion, characterized by a linear decrease above 2 Å. The groups of data points are separated by spaces accordingly to the way as the atoms are distributed as a function of distance.

IV. CONCLUSIONS

A metallic behavior of bulk magnetite in the cubic phase is concluded, whereas the monoclinic phase with $P2/c$ symmetry is characterized by an insulating band gap ($\Delta_g = 0.25$ eV) in agreement with experimental results linked to the Verwey transition. Results evidence that the ground-state cohesive energy is much smaller in the $P2/c$ phase than in the $Fd\bar{3}m$ phase, indicating that the low-temperature monoclinic phase of $P2/c$ symmetry is energetically more stable. Even for clusters, the ground-state phase is that originated from a $P2/c$ structure. This fact suggests that magnetite nanoparticles should, in principle, exhibit Verwey transition. The signature of metallic behavior is still preserved for

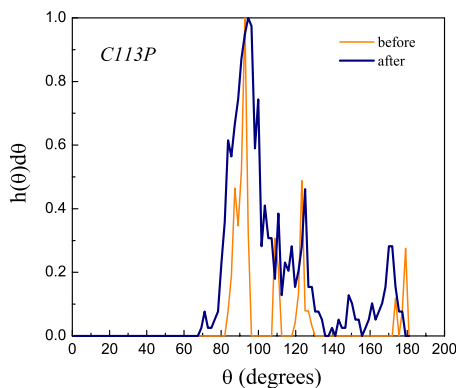


FIG. 12. (Color online) Angular distribution function for $C113P$, before and after relaxation.

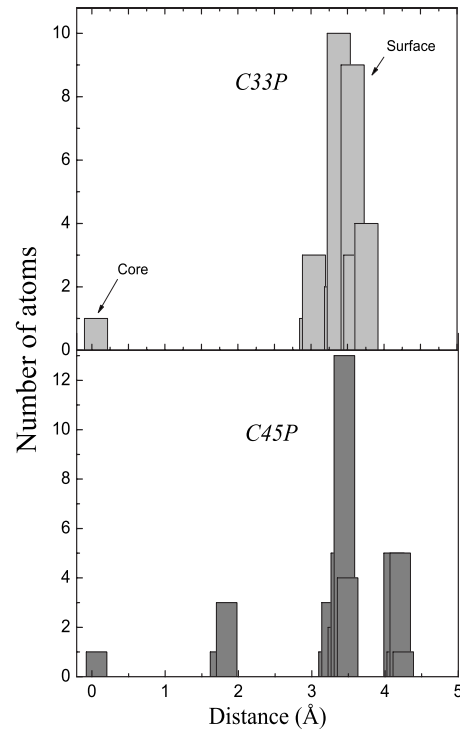


FIG. 13. Distribution of the number of atoms with the distance measured respect to the center of the cluster for $C33P$ (top panel) and $C45P$ (bottom panel).

$C113F$ clusters, resembling a nonstoichiometric magnetite according to its Fe:O proportion, whereas in the case of $C113P$ clusters the width of the band gap in the minority spin channel increases to 0.3 eV reinforcing the onset of an insulating state. The scenario is more complex for smaller clusters as long as the bands are not longer observed and the discrete character of the energy levels becomes dominant. Our ground-state calculations reveal also a partial dimerization on the surface of $C113F$ clusters and six nonequivalent iron sites. The situation is different for $C113P$ clusters characterized by a higher number of nonequivalent Fe sites associated to structural disorder. For $C33$ clusters, independently of the initial structure, the central Fe cation exhibits a loss of charge accompanied by a remarkable increase in the mag-

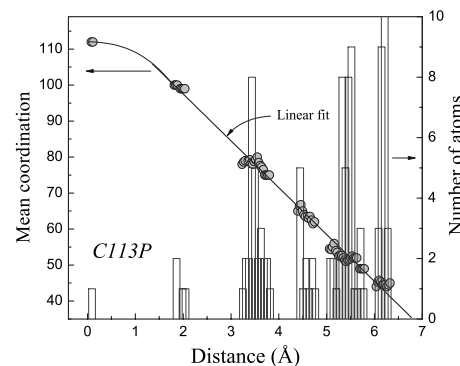


FIG. 14. Distribution of the number of atoms and mean coordination as functions of the distance measured respect to the center of the $C113P$ cluster.

netic moment. For $C33F$ such central moment becomes parallel aligned to those moments of the B sublattice. This alignment is the one responsible for the large value of the magnetization observed for this cluster size and it is related to the weak interaction between the central ion and its surroundings neighbors. Results reveal also a charge transfer process between Fe and O cations characterized by an increase in the electric charge of Fe cations on the surface. Such a charge transfer is also observed in $C45$ and $C113$ clusters. Variations in charge and magnetization were also analyzed as a function of the position of the atoms relative to the center of the clusters. Finally, a structural analysis based on the computation of radial and angular distribution functions as well as on histograms, showing the way as the atoms are located within the clusters, was carried out. In particular, results reveal a peaks broadening in the distribution functions attributed to atomic displacements, respect to the input positions, forming an onionlike structure. Such disorder is however confined to occur in layers of different thickness and caging the central atom. This broadening, which is less

marked in clusters originated from cubic symmetry, agrees with the greater amount of nonequivalent iron sites observed in clusters originated from monoclinic symmetry.

ACKNOWLEDGMENTS

This work was supported by COLCIENCIAS, FONDECYT Grant Nos. 1050066 and 7080111, Millenium Science Nucleus "Basic and applied magnetism" P06-022F, Sostenibilidad projects of the Solid State and the Microelectronic and Scientific Instrumentation Groups of the Universidad de Antioquia, CODI-UdeA project No. IN565CE and PROALMEX Mexico-Germany binational collaboration project. A.H.R. and S.L. were supported by CONACyT México under the Project Nos. J-59853-F, No. J-83247-F, and MICINN of Spain under grant No. MAT2007-65990-C03-03. J.M.Z. is grateful to Universidad de Antioquia and Colciencias for giving support. We also acknowledge the computer time provided by Universidad Politécnica de Valencia as well as CNS, and Ipicyt, México.

*lsinhue@gro.cinvestav.mx

†aromero@gro.cinvestav.mx

‡jmejia@puc.cl

§jomazo@fisica.udea.edu.co

||jrestre@fisica.udea.edu.co

- ¹B. V. Reddy and S. N. Khanna, Phys. Rev. Lett. **93**, 068301 (2004).
- ²B. V. Reddy, F. Rasouli, M. R. Hajaligol, and S. N. Khanna, Chem. Phys. Lett. **384**, 242 (2004).
- ³H. Wu, S. R. Desai, and L.-S. Wang, J. Am. Chem. Soc. **118**, 5296 (1996).
- ⁴L.-S. Wang, H. Wu, and S. R. Desai, Phys. Rev. Lett. **76**, 4853 (1996).
- ⁵D. M. Cox, D. J. Trevor, R. L. Whetten, E. A. Rohlfing, and A. Kaldor, Phys. Rev. B **32**, 7290 (1985).
- ⁶R. L. Whetten, D. M. Cox, D. J. Trevor, and A. Kaldor, Phys. Rev. Lett. **54**, 1494 (1985).
- ⁷D. N. Shin, Y. Matsuda, and E. R. Bernstein, J. Chem. Phys. **120**, 4150 (2004); **120**, 4157 (2004).
- ⁸N. O. Jones, B. V. Reddy, F. Rasouli, and S. N. Khanna, Phys. Rev. B **72**, 165411 (2005).
- ⁹Q. Sun, A. K. Kandalam, Q. Wang, P. Jena, Y. Kawazoe, and M. Marquez, Phys. Rev. B **73**, 134409 (2006).
- ¹⁰Q. Wang, Q. Sun, M. Sakurai, J. Z. Yu, B. L. Gu, K. Sumiyama, and Y. Kawazoe, Phys. Rev. B **59**, 12672 (1999).
- ¹¹Jens Kortus and Mark R. Pederson, Phys. Rev. B **62**, 5755 (2000).
- ¹²Q. Sun, M. Sakurai, Q. Wang, J. Z. Yu, G. H. Wang, K. Sumiyama, and Y. Kawazoe, Phys. Rev. B **62**, 8500 (2000).
- ¹³L. Zhu, K. L. Yao, and Z. L. Liu, Phys. Rev. B **74**, 035409 (2006).
- ¹⁴P. Piekarczyk, Krzysztof Parlinski, and Andrzej M. Oleś, Phys. Rev. Lett. **97**, 156402 (2006); Phys. Rev. B **76**, 165124 (2007).
- ¹⁵Horng-Tay Jeng, G. Y. Guo, and D. J. Huang, Phys. Rev. B **74**, 195115 (2006); Phys. Rev. Lett. **93**, 156403 (2004).

- ¹⁶P. Hohenberg and W. Kohn, Phys. Rev. **136**, B864 (1964); W. Kohn and L. J. Sham, *ibid.* **140**, A1133 (1965).
- ¹⁷S. L. Dudarev, G. A. Botton, S. Y. Savrasov, C. J. Humphreys, and A. P. Sutton, Phys. Rev. B **57**, 1505 (1998).
- ¹⁸J. P. Perdew, J. A. Chevary, S. H. Vosko, K. A. Jackson, M. R. Pederson, D. J. Singh, and C. Fiolhais, Phys. Rev. B **46**, 6671(1992); **48**, 4978(1993).
- ¹⁹P. E. Blöchl, Phys. Rev. B **50**, 17953 (1994).
- ²⁰G. Kresse and D. Joubert, Phys. Rev. B **59**, 1758 (1999).
- ²¹G. Kresse and J. Hafner, Phys. Rev. B **47**, 558 (1993); **48**, 13115 (1993); **49**, 14251 (1994); G. Kresse and J. Furthmüller, Comput. Mater. Sci. **6**, 15 (1996); G. Kresse and J. Furthmüller, Phys. Rev. B **54**, 11169 (1996).
- ²²V. I. Anisimov, I. S. Elfimov, N. Hamada, and K. Terakura, Phys. Rev. B **54**, 4387 (1996).
- ²³V. N. Antonov, B. N. Harmon, V. P. Antropov, A. Ya. Perlov, and A. N. Yaresko, Phys. Rev. B **64**, 134410 (2001).
- ²⁴V. N. Antonov, B. N. Harmon, and A. N. Yaresko, Phys. Rev. B **67**, 024417 (2003).
- ²⁵V. I. Anisimov, J. Zaanen, and O. K. Andersen, Phys. Rev. B **44**, 943 (1991).
- ²⁶G. Henkelman, A. Arnaldsson, and H. Jónsson, Comput. Mater. Sci. **36**, 354 (2006).
- ²⁷H. J. Monkhorst and J. D. Pack, Phys. Rev. B **13**, 5188 (1976).
- ²⁸M. Methfessel and A. T. Paxton, Phys. Rev. B **40**, 3616 (1989).
- ²⁹J. P. Wright, J. P. Attfield, and P. G. Radaelli, Phys. Rev. Lett. **87**, 266401 (2001); Phys. Rev. B **66**, 214422 (2002).
- ³⁰R. Aragón, Phys. Rev. B **46**, 5328 (1992).
- ³¹S. K. Park, T. Ishikawa, and Y. Tokura, Phys. Rev. B **58**, 3717 (1998).
- ³²I. Leonov, A. N. Yaresko, V. N. Antonov, M. A. Korotin, and V. I. Anisimov, Phys. Rev. Lett. **93**, 146404 (2004).
- ³³I. Leonov, A. N. Yaresko, V. N. Antonov, and V. I. Anisimov, Phys. Rev. B **74**, 165117 (2006).
- ³⁴Z. Szotek, W. M. Temmerman, A. Svane, L. Petit, G. M. Stocks,

- and H. Winter, Phys. Rev. B **68**, 054415 (2003).
- ³⁵Z. Lodziana, Phys. Rev. Lett. **99**, 206402 (2007).
- ³⁶N. Guigue-Millot, N. Keller, and P. Perriat, Phys. Rev. B **64**, 012402 (2001).
- ³⁷H. P. Pinto and S. D. Elliot, J. Phys.: Condens. Matter **18**, 10427 (2006).
- ³⁸H. Seo, M. Ogata, and H. Fukuyama, Phys. Rev. B **65**, 085107 (2002).